

Advanced noise modeling for future propulsion systems

International Journal of Aeroacoustics

2018, Vol. 17(6–8) 576–599

© The Author(s) 2018

Article reuse guidelines:

sagepub.com/journals-permissions

DOI: 10.1177/1475472X18789005

journals.sagepub.com/home/jae**Stéphane Moreau¹ and Michel Roger²**

Abstract

In order to meet noise specifications for future foreseen aircraft propulsion systems, such as ultrahigh bypass ratio turbofans and contra-rotating open rotors, the dominant turbomachinery noise mechanisms need to be modeled accurately at an early design stage. Two novel methods are presented here, which could significantly improve the existing analytical noise models. For the high-solidity ultrahigh bypass ratio, a mode-matching technique based on a modal expansion of acoustic and vortical variables in each subdomain of a blade row is shown to accurately reproduce sound generation and propagation in two-dimensional bifurcated channels and in three-dimensional annular unstaggered flat-plate cascades. For the low solidity contra-rotating open rotors, several extensions to Amiet's compressible isolated airfoil theory are coupled with Curle's and Ffowcs Williams and Hawkings' acoustic analogy in the frequency domain within a strip theory framework, to yield both far-field tonal and broadband noise. Including sweep in both tonal and broadband noise models is shown to significantly improve the comparison with experiments on a stationary swept airfoil in a uniform turbulent stream and on a realistic contra-rotating open rotor geometry at approach conditions.

Keywords

Aeroacoustics, propulsion systems, turbofan noise, contra-rotating open rotor noise

Date received: 12 March 2018; accepted: 30 May 2018

Introduction

Even though substantial reductions in aircraft noise have been achieved in recent decades, mostly through the development of increasingly silent engines, continuously growing air

¹Department of Mechanical Engineering, Université de Sherbrooke, Sherbrooke, Canada

²Laboratoire de Mécanique des Fluides et d'Acoustique, University of Lyon, École Centrale de Lyon, Lyon, France

Corresponding author:

Stéphane Moreau, Department of Mechanical Engineering, Université de Sherbrooke, 2500 Blvd de l'Université, Sherbrooke, QC J1K2R1, Canada.

Email: stephane.moreau@usherbrooke.ca

traffic requires further improvements to be made. Fuel burn is an additional concern due to the progressive reduction of natural resources and the increase in atmospheric pollution. Noise and fuel burn thus appear as key factors for the future, to be kept at reasonable levels for minimum noise exposure around airports and pollutant emissions. The next generation of propulsion systems will have to comply with objectives that cannot be specified yet in view of the long development times in aeronautics. This is why, for instance, a sufficient margin has to be maintained in terms of noise to stay below thresholds that are regularly lowered. In this context, two major technologies are identified as good candidates. One is the ultrahigh by-pass-ratio (UHBR) engine, understood as an extension of the existing turbofan engines in which the fan diameter will be increased at the price of a relatively shorter nacelle. The other one is the contra-rotating open rotor (CROR) system ensuring even higher equivalent bypass ratios (BPRs). The first one achieves quite a comfortable acoustic margin of an expected 15–20 dB but with modest fuel burn improvements, whereas the latter could result in up to a 30% fuel burn reduction but with a modest noise margin.¹

Whatever the choice might be, both technologies must be assessed in terms of radiated noise at the early design stage. For this, robust and as accurate as possible prediction tools able to take advanced characteristic features into account are needed. Such features are typically the geometrical parameters involved in the blade design: camber, lean, sweep, and so on. Present strategies based on numerical simulations ensure the accuracy but their computational cost does not allow repeated calculations in optimization algorithms. Furthermore, all geometrical details must be already determined prior to any flow-and-sound computation, which makes them useless when some details are yet to be chosen. Analytical strategies thus appear as an attractive alternative, precisely because they have to ignore details for mathematical tractability. But the involved simplifications in analytical models have to preserve the underlying physics and must be assessed against references of either experimental or numerical nature. Furthermore, they have to stay reliable and extendable when introducing the aforementioned design details to become true design tools.

The present paper is a review of analytical methods aimed at precisely identifying the limitations and possibilities of extensions, in both the UHBR and CROR architectures, focusing only on rotating-blade noise mechanisms. It refers to classes of mathematical formulations in the frequency domain that have been developed in two parallel collaborative industrial chair programs.

Depending on geometrical dimensionless ratios, a blade/vane row can be considered as a cascade or just as a series of isolated airfoils. This leads to quite different approaches as discussed in the next section. One of the key results for cascades in a turbofan noise context presented in a subsequent section is the development of a mode-matching approach for modeling both noise generation and propagation in a blade/vane row. This approach is based on modal expansions in various subdomains of a turbomachine understood as a system of bifurcated waveguides. For the alternative CROR propulsion system, several extensions of existing models for isolated airfoils based on Ffowcs Williams and Hawkings' (FWH) analogy² and the rotating dipole formula are then presented. Typical applications and examples are selected in each case. Some concluding remarks and perspectives are finally drawn in the last section. It must be noted that, for conciseness, as a review of works performed within the framework of special programs by the authors, the present study refers to a nonexhaustive list of references from which the bibliography could be completed.

Dimensional considerations and basic assumptions

Moving/stationary blade/vane rows are characterized by geometrical dimensionless parameters that can help identify the dominant scattering effects or interactions and define suitable modeling approaches. For instance based on the unwrapped representation of an outlet guide vane (OGV) row at radius R_0 , the main dimensions are the chord length c , the solidity $\sigma = cV/(2\pi R_0)$ where V is the vane number, the intervane channel height h and the overlap d related to other parameters by the stagger angle γ defined as the vane angle with respect to the cascade front direction. Different behaviors are expected depending on the values of h/c or d/c and σ . CRORs are characterized by quite large values of h/c or small solidity, with essentially no overlap. In this case, unsteady loadings establish closer to an isolated airfoil model. In ducted propulsion systems (e.g. a turbofan stage) the solidity is quite higher and the overlap d/c is significant, especially for the OGV. Sound waves generated by the interaction mechanisms are partly confined and give rise to a waveguide response inside the intervane channels. This makes sound generation and propagation features hard to separate. Moreover, in ducted systems, an in-duct formulation in terms of propagation modes is already used, which fits quite naturally with a similar description inside the channels. In contrast, open rotors radiate in free field, which now fits better with the single airfoil response.

These considerations first led to define two complementary approaches depending on the ranges of parameters, with asymptotic trends that can be defined as the isolated airfoil range and the cascade range.

The ratios d/c and h/d are displayed as functions of σ for various values of the stagger angle γ in Figure 1. The lines are drawn for values of angle γ that are multiples of 10° . The total colored area corresponds to the domain of possible values. The isolated airfoil response is considered as valid for negative d/c (no overlap) but also, at the price of some approximation, in the upper part of the chart where h/d is large enough. This is highlighted by the green areas. In the remaining gray areas, a cascade response is a priori preferable because of the vicinity of adjacent vanes and/or the degree of overlap.

A second point of interest is the basic mathematical statement required to ensure analytical tractability. First, the main common assumption is that inviscid and linearized equations are considered, essentially in the frequency domain because the involved mechanisms depend on the ratios between the acoustic wavelengths and the aforementioned characteristic dimensions. Therefore, the convected Helmholtz equation is used as a background. Second, as sound is generated by the impingement of incident vortical disturbances on a solid surface, the interaction is much faster than the characteristic lifetime of the disturbances; inertial effects dominate and viscosity does not play a role, except at a trailing edge. According to Chu and Kovászny's³ linearized analysis, the incident vortical motion tends to be frozen and the rigid wall boundary condition on the surface can be fulfilled only if the response of the surface is purely potential. In the case of incident acoustic waves, the diffraction is also a matter of potential response by definition.

These considerations mean that sound generation and sound diffraction by isolated airfoils or cascades can be addressed in the same way within the scope of a linear theory. All models described in the following sections are based on this framework. Viscosity is ignored in the interaction mechanisms, except at the trailing edges where a Kutta condition is imposed for physical consistency.

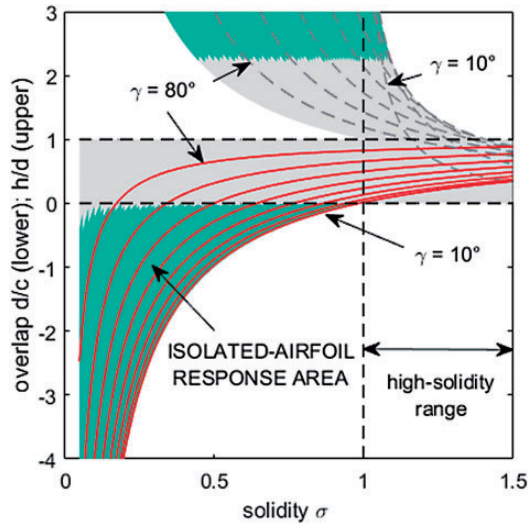


Figure 1. Dimensional analysis of propulsion systems.

Another possible limitation of most analytical formulations is that blades and vanes are modeled as thin flat plates for mathematical simplification, which is hardly compatible with true blade/vane shapes. The zero thickness assumption is acceptable for most fans, open rotors, and compressor stages that need to be addressed in priority for environmental issues and involve thin controlled diffusion airfoils. In contrast, the mean camber of blades/vanes is directly related to the inclination of the equivalent acoustic dipoles in the sense of the acoustic analogy. As such it must be accounted for, especially for OGVs that have to ensure swirl recovery. This is why the possibility of including both stagger angle and camber in analytical models is addressed in the generalized mode-matching section for cascades and in the swept blade section for isolated airfoils.

Turboengine fan noise

Most of the present aircraft propulsion systems involve ducted turbofans where the dominant noise sources with the event of high BPR engines are the jet and the fan in most flight conditions. Until recently the main fan noise source has been the interaction of the fan wakes with the homogeneous downstream OGV. The structural pylon bifurcations (as shown in Figure 2) were enough downstream to have a negligible contribution. Secondary sources involve the fan self-noise, possible inlet turbulence interaction noise, and tip noise. Moreover, in case of incidence, some inlet distortion could induce additional noise sources on the rotor. Yet, the nacelles have been designed to be long enough to mitigate such possible distortion and again limit this additional noise source. Moreover, liners could be placed at the inlet to reduce mainly tonal noise. Yet, with the advent of UHBR engines to further improve fuel efficiency, the nacelles have to be shortened to reduce mass and drag, and the bifurcations have been moved into the OGV row yielding a full

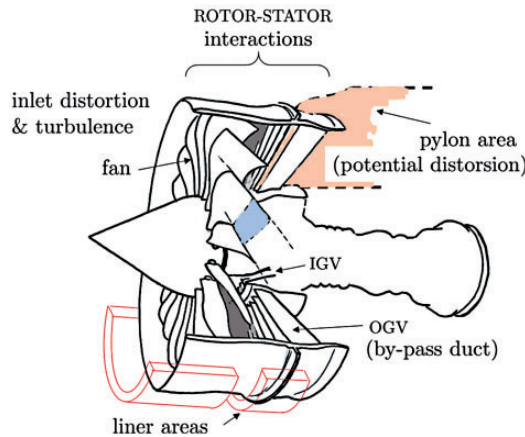


Figure 2. UHBR noise mechanisms. Adjacent blade overlap is featured as the blue area. IGV: inlet guide vane; OGV: outlet guide vane.

heterogeneous vane distribution with strong upstream and downstream flow distortions. Similarly, inlet distortion with incidence will now play a more significant role in noise generation.^{4,5}

Analytical model

Most existing analytical works dedicated to turbomachinery noise rely on the so-called strip theory approach, depicted in Figure 3. The considered fan stage and its surrounding flow are split into annular strips. In a single strip, the mean flow conditions and the geometry are assumed homogeneous along the span, so that the aeroacoustic phenomena are locally described in the unwrapped annulus in Cartesian coordinates, for mathematical tractability. Typically the solution involves a three-dimensional rectilinear cascade response obtained by a Wiener–Hopf method^{6–10} or a single airfoil response such as described in a subsequent section. Yet, only the former respects the criteria in Figure 1 and cascade effects are expected to be significant in turbofans. Spanwise variations in the stage are accounted for by giving adjacent strips different flow conditions and geometrical parameters. The main drawbacks of the approach are that the radial scattering of hydrodynamic or acoustic modes that couple all strips cannot be reproduced on the one hand, and that adjacent vanes are assumed artificially parallel and their response often uncorrelated from strip to strip on the other hand. The latter has been partially addressed by Posson et al.¹¹ by considering a three-dimensional excitation and a three-dimensional blade response in each strip and a cylindrical correction in the rectilinear cascade response. The former modification is the most significant improvement as shown by Grace.¹² Yet, the artificial resonances in the straight channels, already highlighted by Elhadidi and Atassi,¹³ still exist in the model and the radial scattering is still not properly accounted for.

An alternative approach for modeling both noise generation and propagation in a blade row is described in the next section. It can take into account a full three-dimensional annular duct geometry without resorting to strips and therefore naturally accounts for the radial

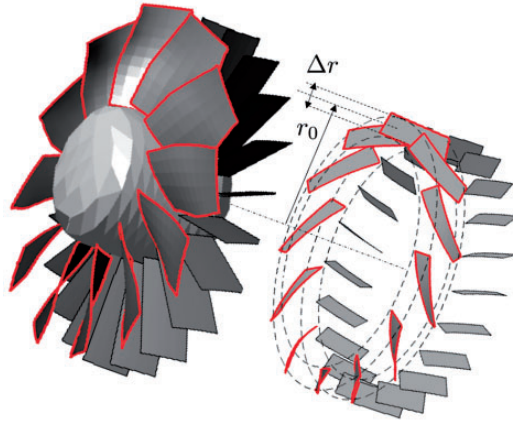


Figure 3. Definition of an annular strip of mean radius r_0 for analytical modeling, assuming homogeneous conditions over the span length Δr .

scattering. The formulation has been implemented for stator scattering of both incident acoustic waves and vorticity waves representative of rotor wake disturbances,^{14,15} as shown later on.

Basic mode-matching procedure

The approach is only described and applied to stator noise in this section,¹⁵ but it could be formulated for a rotor in the rotating reference frame, as well. The main necessary condition is that all vanes substantially overlap as in most OGV designs so that the cascade of vanes can be equivalently considered as a periodic array of bifurcated waveguides, as shown in Figure 4. This allows resorting to classical mode-matching techniques, such as reviewed by Mittra and Lee.¹⁶ For this reason, the approach is referred to as the mode-matching technique in bifurcated waveguides (MMBW). In its three-dimensional version, it is aimed at providing a global account of an annular cascade.

The MMBW technique only assumes that modal expansions of the total disturbance field, including vortical and acoustic waves, are available in each subdomain of space, namely in the present case the annular ducts upstream and downstream of the OGV row and all intervane channels. Once explicit expressions are written for all modes, they are matched at the interfaces in agreement with general gas dynamics conservation laws. This leads to an infinite system of linear equations that is truncated and solved by matrix inversion to determine the coefficients of all waves. The only required information is some prescribed incident acoustic or vortical wave. In the first case, the MMBW technique produces the transmitted and reflected waves. In the second case, it produces the aerodynamically generated waves upstream and downstream. Flow rate and enthalpy conservation are imposed in the OGV case with a uniform axial flow, which is equivalent to the continuity of the acoustic pressure and the total fluctuating axial velocity. A Kutta condition is also considered, stating that the pressure jump between both sides of a vane goes to zero just upstream of the trailing edge. This corresponds to an additional constraint on the modes of

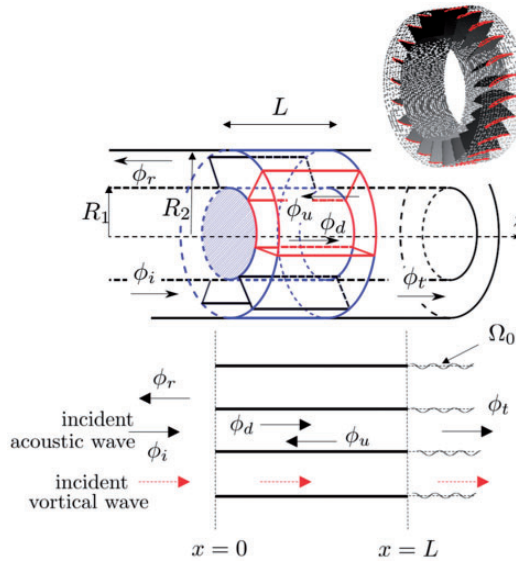


Figure 4. Top: Realistic OGV cascade configuration and its modeling by a zero-staggered annular cascade in uniform axial flow. Potentials of the incident, reflected, transmitted, and upstream-and-downstream channel waves indicated as, respectively, ϕ_i , ϕ_r , ϕ_t , ϕ_u , ϕ_d . Bottom: Two-dimensional formulation featuring ideal wakes. Flow from left to right.

two adjacent channels when solving the matching equations at the trailing edge interface. The linear system resolution provides a uniformly valid description of the sound field as well as modal coefficient spectra.

For simplicity the formalism is only detailed in a two-dimensional framework and for the sound generation problem here (Figure 4, bottom). Complete derivations can be found in François et al.¹⁴ and Bouley et al.¹⁵ The potentials of the incident, reflected, transmitted, and upstream-and-downstream channel waves are termed ϕ_i , ϕ_r , ϕ_t , ϕ_u , ϕ_d , respectively. Let an incident oblique hydrodynamic gust be specified by its velocity, replacing the incident potential ϕ_i that would describe an incident acoustic wave. The hydrodynamic velocity is expressed by its streamwise (v_x) and normal (v_y) components, as

$$(v_x, v_y) = w_n e^{inBy/r_0} e^{inB\Omega x/U_0} \left(1, -\frac{\Omega r_0}{U_0} \right) \tag{1}$$

in order to ensure its incompressible property. Here B is the number of blades or wakes, y is the tangential coordinate, Ω is the rotational speed, and w_n is the amplitude. This incident field has to be continued as a frozen pattern in other subdomains such that the potential response of the cascade can be derived. This requires a special modal expansion inside the intervane channels in the form

$$(v_x, v_y) = e^{inB\Omega x/U_0} \times \sum_{j=0}^{\infty} A_j^{(0)} \left(\cos[j\pi y/a], -i \frac{nB\Omega a}{j\pi U_0} \sin[j\pi y/a] \right) \tag{2}$$

the superscript (0) referring to the reference channel and a phase shift e^{imu} being introduced for the m th adjacent channel, where $u = 2\pi nB/V$, V being the number of vanes. $a = 2\pi r_0/V$ is the channel width. The potentials associated with the generated acoustic waves are written as

$$\phi_r = \sum_{s=-\infty}^{\infty} R_s e^{i\alpha_{r,s}y} e^{iK_{r,s}^-x}, \quad x < 0 \quad (3)$$

$$\phi_t = \sum_{l=-\infty}^{\infty} T_l e^{i\alpha_{t,l}y} e^{iK_{t,l}^+x}, \quad x > L \quad (4)$$

with $\beta^2 = 1 - M_0^2$ and

$$\alpha_{r,s} = \frac{nB + sV}{r_0}, \quad \beta^2 K_{r,s}^- = -M_0 k_n - \sqrt{k_n^2 - \beta^2 \alpha_{r,s}^2}$$

$$\alpha_{t,l} = \frac{nB + lV}{r_0}, \quad \beta^2 K_{t,l}^+ = -M_0 k_n + \sqrt{k_n^2 - \beta^2 \alpha_{t,l}^2} \quad (5)$$

$$(\phi_u^{(m)}, \phi_d^{(m)}) = \sum_{q=0}^{\infty} (U_q^{(0)} e^{iK_q^-x}, D_q^{(0)} e^{iK_q^+x}) e^{imu} \cos\left(\frac{q\pi}{a}y\right)$$

with $\beta^2 K_q^\pm = -M_0 k_n \pm \sqrt{k_n^2 - \beta^2 \left(\frac{q\pi}{a}\right)^2}$ from which the pressure and velocity are obtained. In the case of an incident acoustic wave a unit initial potential is specified as $\phi_i = e^{iny/r_0}$ to ensure the periodicity condition of an unwrapped duct mode, and no vortical mode is to be considered inside the channels.

The last point still required to close the problem is the Kutta condition, expressing that the pressure inside adjacent channels is the same on both sides of their common wall just at the trailing edge. It leads to the additional equation

$$\sum_{q=0}^{\infty} (k - K_q^- M_0) [1 - (-1)^q e^{-iu}] U_q^{(m)} = - \sum_{p=0}^{\infty} (k - K_p^+ M_0) [1 - (-1)^p e^{-iu}] D_p^{(m)} e^{iK_p^+ L} \quad (6)$$

that induces an overdetermination of the system of equations. Now the Kutta condition also results in the shedding of concentrated vorticity in the vane wakes. The intensity Γ_0 of this vorticity is an additional variable, so that a well-posed problem is finally obtained, with another equation

$$\sum_{q=0}^{\infty} [K_q^+ D_q^{(0)} e^{iK_q^+ L} + K_q^{(-)} U_q^{(0)}] \varphi_{\nu,q} = K_\nu^+ T_\nu a + \frac{\alpha_\nu \Gamma_0}{\alpha_\nu^2 + (\omega/U_0)^2} \quad (7)$$

involving the scalar product

$$\varphi_{\nu,q} = \int_0^a e^{-i\alpha_\nu y} \cos(\alpha_q y) dy$$

Solving of the matrix of equations generated by the conservation laws at the interfaces yields all coefficients R_s , T_σ , U_q , D_q , Γ_0 up to the specified truncation orders. The acoustic powers transmitted upstream and downstream are then deduced from classical definitions. The same procedure is extended in a three-dimensional context with annular duct modes instead of oblique plane waves and cosine-Bessel channel modes instead of the cosine modes.

Typical results are summarized in Figure 5 where three-dimensional analytical predictions with the MMBW technique are compared to numerical simulations with the IDDES approach and assessed against in-duct measurements. IDDES provides either a direct simulation (dashed line) or vane pressure fluctuations as input for classical Curle's analogy (cont. line). The measurements have been performed on the ducted ECS fan test bench of the IDEALVENT project.¹⁷ The small-size, low-speed fan is a rotor/stator stage used for aircraft air-conditioning that radiates both tonal noise because of the periodic blade/vane interactions and broadband noise associated with turbulence. The measured data are produced by a multiport technique.¹⁸ Inlet (upstream) and outlet (downstream) power spectra are shown in Figure 5. The red symbols stand for analytical wake interaction broadband noise predictions only, because this mechanism is recognized as dominant. The model is fed with measured turbulent intensity and integral length scales. The overall agreement with the measurements is encouraging, at least in the low-frequency range, here below 3 kHz. Furthermore, the analytical prediction performs almost as well as the numerical simulations (blue lines in the figure, detailed in the reference) that also include other possible broadband noise mechanisms.

It must be noted that the actual stagger angle of the vanes is ignored in this preliminary implementation and that the plane wave mode cannot be excited as a consequence of the zero-stagger assumption.¹⁹ Therefore, some physical aspects are still missing. Yet the results in Figure 5 show that the technique is a promising low-cost alternative. Improvements are shortly described in the next section.

Generalized mode-matching technique

Assuming thin flat plates instead of true curved vanes raises the question of the equivalent stagger angle to be given to the plates. Choosing the true vane angle either at leading edge or at trailing edge produces quite different results.¹⁹ The flat plate model also enforces the same mean flow speed and direction upstream and downstream of the stator, so that the flow is consistently either uniformly axial or with uniform swirl depending on the choice, unlike what is encountered in a real rotor/stator stage. The predictions are questionable for both reasons. In principle, different mean flow conditions could be considered on both sides of a matching interface, as discussed by Roger et al.²⁰ but a substantial ambiguity remains in the definition of relevant matching conditions. The flat plate assumption has to be released so that the swirl recovery that restores an axial flow downstream of the OGV from a swirling flow upstream is reproduced.

The generalized mode-matching technique as proposed by Roger and François¹⁹ is a way of approximately solving the ambiguity. It introduces the curved mean camber line of the vanes in the formulation, as follows. The tangent to the mean camber line at leading edge of angle χ_{LE} is used to define a staggered array of semi-infinite plates on the interface of which the matching procedure is applied. This generates initial modes in the inlet triangle ABC in Figure 6. An arc connecting point C to the trailing edge is used to complete the channel, the

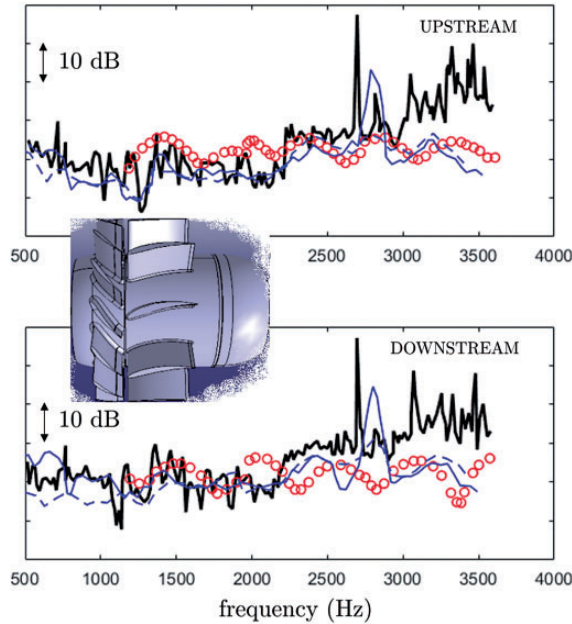


Figure 5. In-duct measured power spectra for the rotor/stator ECS fan tested in IDEALVENT¹⁷ (black). Analytical predictions with the MMBW technique as red symbols. Blue lines stand for IDDES-based numerical simulations, either direct (dashed) or indirect (plain; Curle's analogy).

lower wall of which does not coincide anymore with the mean camber line. This artificially restores some consistent vane thickness in the model. The initial solution taken in the oblique cross-section BC of height h_i is then used as input in a slowly varying duct transmission model, ignoring the curvature but accounting for the associated continuous enlargement, according to Rienstra's formulation.²¹ This is equivalent to consider that the channel only acts as a straight diverging duct. The standard mode-matching procedure of the previous section is applied next on the trailing edge interface of height h_0 where the local stagger angle is zero. Though approximate, this statement allows including vane curvature in the MMBW technique and produces a uniformly valid description of the acoustic field with a realistic, continuous mean flow deviation. Its simplicity makes it a good candidate for both tonal and broadband noise predictions. In principle the varying cross-section of the intervane channel makes cuton-to-cutoff and cutoff-to-cuton transitions take place for some modes at some locations, which could be accounted for by using Ovenden's regularization.²²

Sample results are shown in Figure 7(a) on the NASA-SDT test case. The transmission of the angular mode -12 in the reference configuration with 54 stator vanes is considered in an unwrapped cut at mid-span. Therefore, only nine vanes are shown, which fits with two tangential wavelengths of the incident mode. The test corresponds to the approach condition at axial Mach number 0.4. In the analytical model, the vanes are replaced by zero thickness curved plates so that the curvature of the intervane channel and its expansion from upstream to downstream is reproduced. As a result, the downstream axial speed differs from

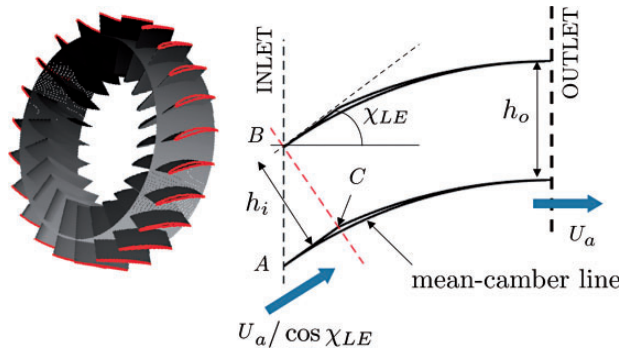


Figure 6. Definition of the bent intervane channel seen as a waveguide, with inlet and outlet interfaces for the matching. Case of constant axial velocity U_a .

the upstream one, leading to the change of wavefront angle featured by the dashed lines. The acoustic field is continuous. Only the same mode -12 is cuton in the scattered field in this example; therefore, regular wavefronts are expected downstream. Interference patterns are seen upstream where the reflected mode combines with the incident mode. The same case as numerically simulated by Hixon²³ with the BASS code is reported in Figure 7(b). The same qualitative sound field is obtained, except that the additional interference patterns downstream of the cascade are attributed to spurious reflections on the right side boundary of the computational domain. Fine details of the wave transmission such as those caused by the true mean flow gradients and vane shape are ignored in the analytical model but the dominant features are reproduced. The model provides an approximate but physically consistent description of the acoustic field, with a negligible computational time. This makes it an attractive candidate to be included in a fast-running prediction tool. Further developments are in progress to extend the method to a three-dimensional annular cascade.

CROR noise

In the field of unducted propulsion systems, CRORs are also identified as an alternative ensuring equivalent UHBR and better propulsive efficiency. Yet, they radiate high-level noise and often high-amplitude tones. The main flow features responsible for such a nuisance are summarized in Figure 8 for the most common pusher configuration. First, the airflow incidence on the CROR affects all rotor sources. Then the pylon viscous wake interacts with the front rotor and possibly with the rear rotor if its velocity deficit is still deep enough. Pylon/front rotor forward and rearward potential field interactions also take place. Both rotors yield rotor-alone tones caused by thickness and loading noise, the former being important at high speeds. The front rotor sheds viscous wakes that interact with the aft rotor. Its tip vortex can also interact with the aft rotor in flight configurations yielding a significant *vena contracta*, even if the aft rotor is cropped. There are also rotor/rotor forward and rearward potential field interactions. The sources colored in red in Figure 8 are generally the dominant external noise sources in such a propulsion architecture, which combine with the core engine sources in black. Those in blue and brown can also be significant in certain flight configurations. Only the green ones can generally be neglected as the distances between the various components are large enough. The rotor/rotor viscous wake interaction

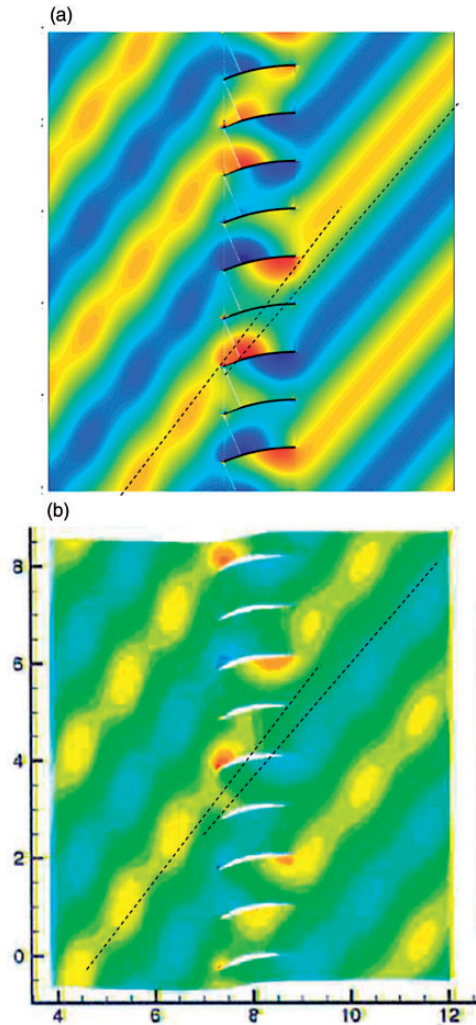


Figure 7. Instantaneous pressure maps for the transmission of an oblique wave through the NASA SDT test case cascade. (a) Mode-matching technique and (b) numerical simulation with the code BASS, from Hixon.²³

and the tip vortex interaction can be seen as CROR-alone noise sources, whereas the pylon/rotor viscous wake interaction and airflow incidence are rather installation effects.

The above noise mechanisms contribute to both tonal and broadband noise. The former can be predicted by unsteady Reynolds-Averaged Navier–Stokes (u-RANS) simulations. Such simulations have been first achieved on the stand-alone CROR for which single blade passages can be used, limiting the model size.^{24–26} More recently full configurations have also been considered when installation effects such as the pylon need to be accounted for.²⁷ Yet, even for approach conditions for which the Reynolds numbers are lower, the grid size is always large and typically involves more than five million points. Therefore, even if significant progress has been made in the prediction of tonal noise, the computational cost

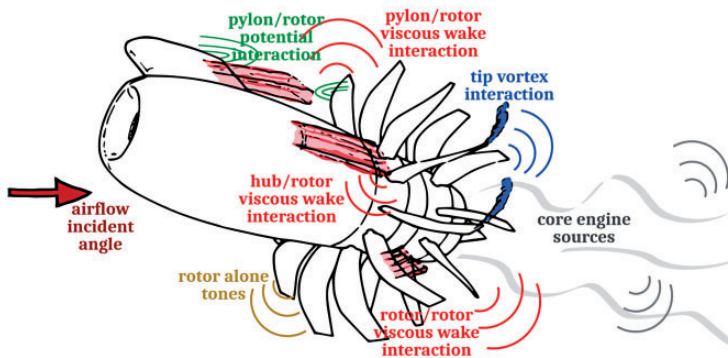


Figure 8. CROR noise mechanisms.

is still high and can hardly be included in an optimization loop.²⁸ Actually, most of the shape optimization efforts have been put both numerically and experimentally on the CROR-alone configuration (see, for instance the DREAM project results²⁹), even though the installation effects are known to increase the overall noise significantly. These optimizations are also often limited to low-speed cases as recently performed by Grasso,³⁰ on the VKI L1 wind-tunnel CROR. Moreover, the numerical prediction of the broadband noise component of the CROR requires simulating significant turbulent scales in the flow over the blade surfaces and in their wake. A Large Eddy Simulation (LES) of even a single CROR blade is still prohibitively expensive because of the blade size and the high chord-based Reynolds number involved. Therefore, fast prediction methods able to include technological features such as blade sweep, hub–blade junction, and blade tip effects are still needed as guidelines for low-noise design.

Most analytical CROR noise modeling again relies on the strip theory approach^{31,32} illustrated in Figure 3. Such a method is also retained here, and both rotors and their surrounding flow are split into annular strips in which the mean flow conditions are assumed homogeneous. When the criteria in Figure 1 are applied to a typical CROR geometry, the solidity and overlap ratio strongly suggest an isolated airfoil response. Amiet^{33,34} has proposed both a leading edge and a trailing edge compressible noise model valid for any Mach number and high frequencies. Several extensions of these edge models have been proposed and summarized by Roger and Moreau,³⁵ to account not only for trailing edge self-noise and turbulence interaction noise but also for the vortex shedding noise, and to account for noncompact finite chord effects by introducing second-order backscattering terms. The latter corrections have also extended the frequency range of the original models.³⁶ Yet, they all involve straight edges that are not representative of modern CRORs. Moreover, only two broadband noise mechanisms can be addressed with the above isolated airfoil responses, namely self-noise from both rotors and the turbulence-impingement noise from the front rotor wake. Two extensions are then presented below as examples.

Turbulence-impingement noise on a swept airfoil

A first extension of Amiet's theory for CROR has been to account for sweep.^{37–40} Other ones have been to generalize the former to any trapezoidal segment,⁴¹ and then to account

for tip effects, first in the limited case of a flow parallel to the blade tip⁴² and more generally in the presence of a *vena contracta*.⁴³ To illustrate these extensions only the sweep effect is considered here. The airfoil is assumed as an infinitely thin flat plate of finite chord length to yield an analytical solution of the linearized Euler equations reformulated into a convective wave equation. For the prediction of broadband turbulence interaction noise, the turbulence is assumed frozen and isotropic, and expanded into harmonic gusts. In its more general three-dimensional form the theory involves both efficient, supercritical gusts and poorly efficient subcritical gusts, both kinds of gusts corresponding to either supersonic or subsonic phase speeds of the interaction along the leading edge, respectively. The analytical prediction of the unsteady loads induced by grid-generated turbulence on such a swept flat plate is then used to calculate the far-field sound spectrum. The general expression of the power spectral density (PSD) of the far-field acoustic pressure in a fluid of density ρ_0 and speed of sound c_0 involves an integral over all spanwise wavenumbers. It reads for a far-field observer at \mathbf{x} and an angular frequency ω

$$S_{pp}^\psi(\mathbf{x}, \omega) = \left(\frac{k\rho_0 x_3}{2S_0^2} \right)^2 U_1 \pi \frac{L}{2} \int_{-\infty}^{\infty} \Phi_{ww} \left(\frac{\omega - k_2 U_2}{U_1}, k_2 \right) \left| \mathcal{L} \left(x_1, \frac{\omega - k_2 U_2}{U_1}, k_2 \right) \right|^2 \Sigma^2 dk_2 \tag{8}$$

with

$$\Sigma^2 = \frac{\sin^2 \left[\left\{ \frac{1}{\beta_0^2} \left(k\beta_1^2 \frac{x_2}{S_0} - M_2 \right) - k_2 \right\} \frac{L}{2} \right]}{\left[\frac{1}{\beta_0^2} \left(k\beta_1^2 \frac{x_2}{S_0} - M_2 \right) - k_2 \right]^2}$$

$k = \omega/c_0$ is the acoustic wavenumber. Φ_{ww} is the two-wavenumber spectrum of the velocity component normal to the airfoil and \mathcal{L} an analytical aeroacoustic transfer function or radiation integral.⁴² U_j ($j = 0, 1, 2$) denotes the velocity components in Figure 9, M_j the corresponding Mach number, and $\beta_j^2 = 1 - M_j^2 \cdot (x_1, x_2, x_3)$ are the streamwise, normal spanwise, and perpendicular observer coordinates, with $S_0^2 = x_1^2 + \beta_0^2(x_2^2 + x_3^2)$ the observer distance accounting for convection effects. $k_1 = \omega/U_0$ and k_2 are the streamwise and normal spanwise wavenumbers. c and L are the chord and span indicated in Figure 9.

Under the assumption of large aspect ratio, typically valid beyond $L/c > 3$, the result is more simply expressed as

$$S_{pp}^\psi(\mathbf{x}, \omega) \simeq \left(\frac{k\rho_0 x_3}{2S_0^2} \right)^2 U_1 \pi \frac{L}{2} \Phi_{ww} \left(\frac{\omega - K_2 U_2}{U_1}, K_2 \right) \left| \mathcal{L} \left(x_1, \frac{\omega - K_2 U_2}{U_1}, K_2 \right) \right|^2 \tag{9}$$

with

$$K_2 = \frac{k}{\beta_0^2} \left(\beta_1^2 \frac{x_2}{S_0} - M_2 \right)$$

and it can be verified that the only involved gust (corresponding to K_2) is always supercritical. For supercritical gusts, the radiation integral $\mathcal{L} = \mathcal{L}_1 + \mathcal{L}_2$ is the sum of two

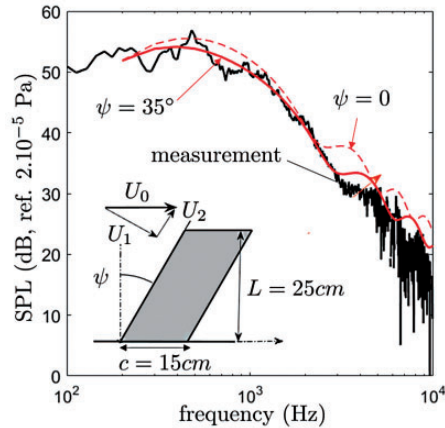


Figure 9. Far-field noise spectrum of turbulence-impingement noise on a swept airfoil (50 m/s). Comparison with predictions ignoring (thin dashed) and accounting for (plain) sweep. SPL: sound pressure level.

contributions from the leading edge scattering and the trailing edge scattering, respectively. As shown, for instance by Giez et al.,³⁹ both radiation integrals involve the sweep angle ψ . As ψ goes to zero the classical expressions for a rectangular unswept airfoil are recovered.³⁵

A recent experiment in the large open-jet anechoic wind tunnel at École Centrale de Lyon (ECL) has been achieved on a thin swept and loaded airfoil to confirm the effect of sweep and validate the above broadband noise model. In this experiment shown in Figure 10 the extruded airfoil is mounted vertically in a rotating disk inserted in a large horizontal plate at the exit of a nozzle with a 300 mm by 400 mm rectangular section. It is placed in a quasi-homogeneous grid-generated turbulence of 8% intensity. The flow velocity has been varied up to 110 m/s, which corresponds to a Mach number of about 0.3.³⁹

Predictions were made using two versions of the above model, with zero sweep and with the actual 35° sweep in equation (8), respectively. A von Kármán spectrum has been fitted to the measured velocity spectrum at the airfoil leading edge location. Sample results are shown in Figure 9 for a velocity of 50 m/s and a far-field microphone at 90° from the flow direction in the mid-span plane. Accounting for sweep in the model reproduces much more accurately the overall sound level, as well as the high-frequency humps and dips of the sound spectrum attributed to noncompactness. The key point, apart from the reduced radiating efficiency inherent to the lower normal velocity (U_1 instead of U_0), is the shifted threshold between supercritical and subcritical gusts when sweep is considered (see, for instance Figure 15 in Quaglia et al.⁴⁰).

CROR tonal noise

The next extension has been to account for the blade sweep in the radiated tonal noise of a CROR with B_1 front blades spinning at Ω_1 and B_2 aft blades spinning at Ω_2 , for both wake interaction and tip vortex interaction noise mechanisms. The main geometrical parameters of these interactions are summarized in Figure 11. Indices 1 and 2 refer to the front and aft

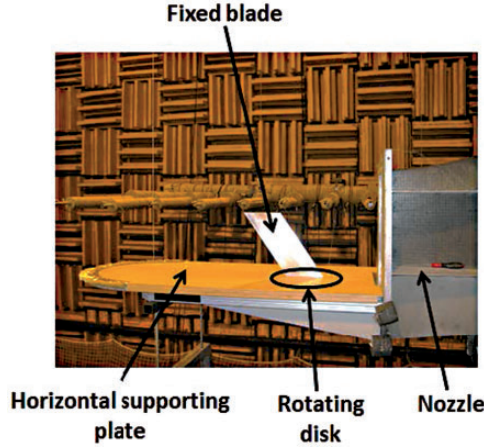


Figure 10. Swept airfoil experimental setup in the ECL large open-jet anechoic wind tunnel.

rotors, respectively. The far-field acoustic pressure p can be obtained using a frequency-based rotating dipole formulation of the FWH equation for CROR including radial forces and forward flight at zero incidence. The noncompact formulation both in chord and span from Hanson and Parzych⁴⁴ is used, in which only the dipolar loading term is kept. For an observer at $\mathbf{x} = (R, \Theta, \Phi)$ and for an interaction frequency $\omega_{mn} = mB_1\Omega_1 + nB_2\Omega_2$ (n and m integers) it reads

$$p(\mathbf{x}, \omega_{mn}) = \int_{\Sigma_r} \frac{-B_2 k_{mn} e^{ik_{mn}(R_e - x_s \cos\Theta_e/D_c)}}{4\pi S_0} \sum_{n=-\infty}^{+\infty} e^{i\chi_{mn}(\phi_s - \Phi - \pi/2)} \times \left\{ \tilde{P}_{r,m} \frac{\sin\Theta_e}{D_c} J'_{\chi_{mn}} \left(\frac{k_{mn} r_s \sin\Theta_e}{D_c} \right) + i \left[\tilde{P}_{\phi,m} \frac{\chi_{mn}}{k_{mn} r_s} - \tilde{P}_{x,m} \frac{\cos\Theta_e}{D_c} \right] J_{\chi_{mn}} \left(\frac{k_{mn} r_s \sin\Theta_e}{D_c} \right) \right\} d\Sigma_r \quad (10)$$

with $\chi_{mn} = nB_2 - mB_1$ and $k_{mn} = \omega_{mn}/c_0$, the acoustic wavenumber. Σ_r is the aft rotor mean camber surface. S_0 is again the distance to the observer corrected for the convection velocity U_X (see Figure 11(b)). R_e and Θ_e are the emission coordinates. $D_c = (1 + M_X \cos\Theta_e)$ is the Doppler factor. J and J' denote the Bessel function of the first kind and its derivative, respectively. $(\tilde{P}_{r,m}, \tilde{P}_{\phi,m}, \tilde{P}_{x,m})$ are the Fourier coefficients of the cylindrical components of the unsteady loading on the aft blade. All other geometrical parameters are defined in Figure 11.

In equation (10) the loading components on the aft rotor correspond to wall pressure fluctuations induced by either the front rotor wakes (wake blade interaction (WBI)) or the front rotor tip vortex (orthogonal blade-vortex interaction (OBVI)). In both cases, the pressure jumps are provided by the analytically extended Amiet's response to a harmonic gust on a swept blade segment.^{40,41} The upwash velocity (or normal velocity to the flat plate) is expanded in two-dimensional gusts in the reference frame of the strip segment as detailed in Roger et al.,⁴² for instance. The sweep angle ψ also appears explicitly in equation (10) when integrating over the parallelogram of a given blade strip (see,

for instance equation (20) in Roger et al.⁴² or equation (27) in Quaglia et al.⁴⁰ for the OBVI mechanism).

Finally, note that for tonal noise applications from large blades of open rotors the unsteady lift distribution acting as sources is both fully correlated over the blades and acoustically noncompact. Care must then be taken in the application of the above strip theory that would lead to artificial phase and amplitude discontinuities between adjacent blade segments yielding erroneous interferences. For these reasons Carazo et al.⁴⁵ proposed a strip-by-strip interpolation that generates a continuous source distribution over the mean camber surface S_r . Similar caution has been taken by Quaglia⁴³ for the OBVI mechanism.

The validation of the above model is achieved on the FL05/AL05 CROR configuration considered numerically by Soulat et al.²⁶ and tested in the NASA LSWT wind tunnel. It corresponds to an approach condition for which the *vena contracta* yields tip vortex interaction even though the aft rotor is cropped. This CROR case has $B_1 = 12$ front blades and $B_2 = 10$ aft blades, and both rotors rotate at the same absolute speed but in opposite directions ($\Omega_1 = -\Omega_2 = 827$ r/min). Soulat et al. showed that most interaction tones were predicted accurately by combining the u-RANS simulation results with a FWH analogy, as shown by the solid red lines compared with the experimental square symbols in Figure 12 for the two main interaction tones $BPF_1 + BPF_2$ and $BPF_1 + 2 BPF_2$. The two noise mechanisms WBI and OBVI are then considered separately. The tip vortex is first extracted from the

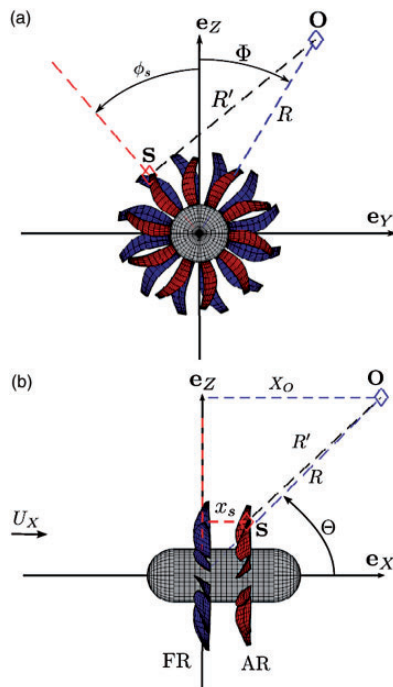


Figure 11. Observer (O) reference frame and main geometric parameters for tonal noise predictions. (a) Front view and (b) side view.

simulation and fitted with a Batchelor vortex model (a Lamb–Oseen model in the vortex tangential plane with an additional Gaussian-shape axial velocity), which was found to closely represent the evolution of the actual front rotor tip vortex.^{43,46} The tip vortex is then subtracted from the shear flow to yield the front rotor wake only. Both contributions are then evaluated and compared to experimental results in Figure 12. The OBVI mechanism is clearly the dominant contributor for both interaction tones. Yet, in some directions and particularly for $BPF_1+2 BPF_2$, the WBI must also be accounted for to reproduce the observed directivity. Both contributions are then summed (black solid lines) to provide a good agreement with the experiment. Similar results are found for the other dominant BPFs and interaction tones.

CROR broadband noise

The final extension has been to account for the blade sweep in the broadband noise model of the same CROR for the wake interaction mechanism (broadband rotor wake interaction or BRWI). The starting point is again the frequency-based rotating dipole formulation of the FWH equation for CROR including radial forces and forward flight at zero incidence, but for a nonperiodic interaction. Equation (10) then reads in a more general form

$$p(\mathbf{x}, \omega) = \int_{\Sigma_r} \frac{-B_2 k e^{ik(R_c - x_s \cos \Theta_e / D_c)}}{4\pi S_0} \sum_{n=-\infty}^{+\infty} e^{in(\phi_s - \Phi - \pi/2)} \\ \times \left\{ \tilde{P}_r(\omega_n) \frac{\sin \Theta_e}{D_c} J'_n \left(\frac{kr_s \sin \Theta_e}{D_c} \right) + i \left[\tilde{P}_m(\omega_n) \frac{n}{kr_s} - \tilde{P}_x(\omega_n) \frac{\cos \Theta_e}{D_c} \right] J_n \left(\frac{kr_s \sin \Theta_e}{D_c} \right) \right\} d\Sigma_r \quad (11)$$

with $\omega_n = \omega \pm n\Omega_2$. Because the noise sources are turbulent and thus random, a statistical processing of this acoustic pressure is needed to yield a PSD S_{pp} as in the above swept airfoil case. The impinging turbulence is again assumed frozen and isotropic, and decomposed into harmonic gusts. All calculations done, the PSD of the far-field acoustic pressure for an observer at $\mathbf{x} = (R, \Theta, \Phi)$ and for a frequency ω reads

$$S_{pp}(\mathbf{x}, \omega) = \frac{\pi B_2 \rho_0^2 B_1^2 k^2}{2S_0^2} \sum_{n=-\infty}^{+\infty} \sum_{m=-\infty}^{+\infty} \int_{r_0 - \Delta r/2}^{r_0 + \Delta r/2} U_{x2} \cos \psi D_{mn}^2 e^{i \tan \psi (K_{x,n} + \kappa_n)(r - r_0)} \\ \times \Phi_{wr}(\mathbf{K}'_s, \omega) \left| \mathcal{L}_n(\mathbf{K}'_s, \omega) \right| dr \quad (12)$$

where D_{mn} is a directivity factor that depends on χ_1 and χ_2 the front and aft rotor mean stagger angles in the strip, respectively. Δr and r_0 are the strip parameters defined in Figure 3. $\mathbf{K}'_s = (K_{x,n}, 0, -\tan \psi (K_{x,n} + \kappa_n))$ is the wavenumber of the incident gust modified by the sweep ($K_{x,n} = \omega \pm n\Omega_2 / U_{x2}$ and $\kappa_n = \pm n \sin \chi_2 / r_{ST} + k \cos \chi_2 \cos \Theta_e / D_c$ are two convective wavenumbers). Similarly the acoustic transfer function is also modified by the sweep

$$\mathcal{L}_n(\mathbf{K}'_s, \omega) = \int_{-b_2/\cos \psi}^{b_2/\cos \psi} g(\cos \psi \xi, \mathbf{K}'_s, \omega \pm \Omega_2) e^{-i\kappa_n \xi} d\xi$$

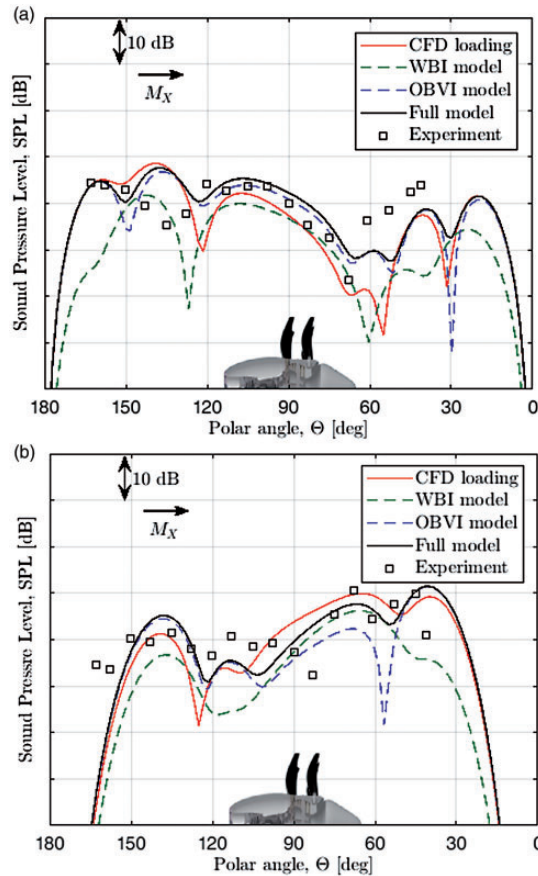


Figure 12. Far-field noise directivity for two interaction tones of the FL05/AL05 CROR approach configuration. Comparison between experiment (square symbols) and predictions considering the WBI only (green dashed), considering the OBVI only (blue dashed) and accounting for both mechanisms (black solid). (a) BPF_1+BPF_2 and (b) $BPF_1+2 BPF_2$. CFD: Computational Fluid Dynamics (u-RANS); OBVI: orthogonal blade-vortex interaction; WBI: wake blade interaction.

where $b_2 = c_2/2$ is the aft rotor half-chord. Equation (12) represents a generalization of the result by Blandeau and Joseph⁴⁷ and Blandeau et al.⁴⁸ that can be retrieved by setting $\psi = 0$.

Note that the poor coherence of the turbulent field and the statistical averaging makes the spanwise continuity of the phase and amplitude of the blade response less critical, and the strip-by-strip interpolation used in the tonal case no longer needed.

The validation of the model was first assessed with Blandeau's canonical blade configuration by Quaglia et al.⁴⁶ The model has then been applied to the above realistic FL05/AL05 CROR approach configuration, using the turbulent variables of the u-RANS simulation to reconstruct a von Kármán spectrum for the front rotor wake impinging turbulence. Figure 13 shows the PSD of the acoustic pressure at distance $R = 20$ m in two directions, upstream of the CROR ($\Theta = 150^\circ$) in Figure 13(a) and above the CROR ($\Theta = 90^\circ$) in Figure 13(b). Good agreement with the experiment is found at frequencies higher than 1 kHz. At lower frequencies the discrepancy is most likely caused by the additional blade trailing edge noise

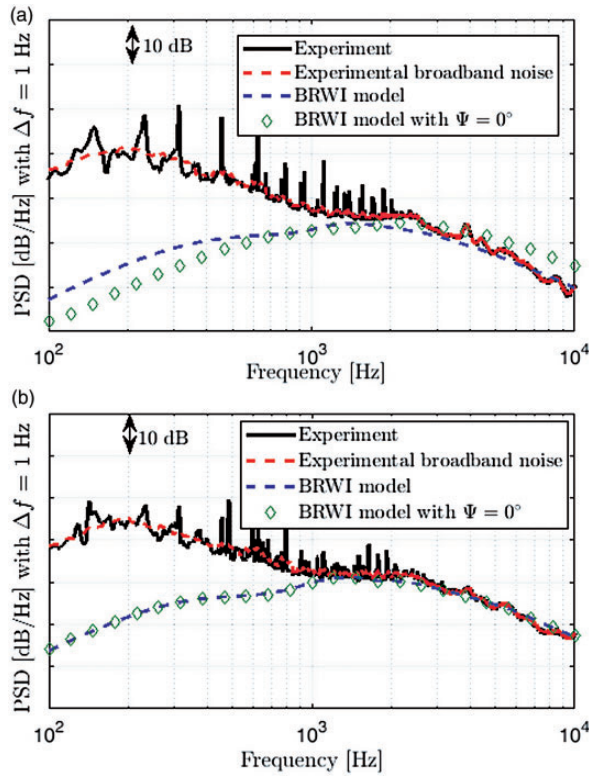


Figure 13. Far-field noise spectra at a distance $R = 20$ m for the FL05/AL05 CROR approach configuration. Comparison between experiment (black solid for full spectrum and red dashed for the broadband component only) and predictions considering the BRWI only: with (blue dashed) and without (diamond symbols) sweep. (a) $\Theta = 150^\circ$ and (b) $\Theta = 90^\circ$. BRWI: broadband rotor wake interaction.

not accounted for in the present calculation, as was found previously by Blandeau et al.⁴⁸ in a different CROR geometry. Accounting for the sweep significantly improves the prediction in the upstream direction.

Conclusions

Future propulsion systems such as UHBR and CROR will face the challenge of better predicting rotating blade noise mechanisms at the design and optimization stages to meet future noise regulations and achieve significant noise reduction. Turbomachinery noise involves both tonal and broadband noise components that need to be both predicted in most flight conditions and particularly at the three certification points. By design, these new propulsion systems will also involve reduced lined areas, which make the integration of acoustic predictions at predesign even more mandatory. Even though numerical simulations are now able to directly predict tonal noise in the most realistic and complex turbofan configurations,⁵ and more recently to predict the fan-OGV broadband noise component,^{49,50} they rely on existing geometries and are still computationally intensive and consequently costly. They can hardly be included in an optimization loop, which drives the need

for advanced analytical noise modeling. Novel aeroacoustic models for future propulsion systems should be capable of addressing sound generation and propagation. They should be applicable to novel integration of these systems with fully asymmetric configurations and account for their blade design. Two such methods have been presented here.

For UHBR turbofans characterized by high-solidity overlapping blade rows, a novel mode-matching technique is proposed to remove some of the existing limitations of current methods based on strip theory and rectilinear cascade responses of infinitely thin flat plates. This method is based on a modal expansion of acoustic and vorticity variables in each subdomain of a blade row. A matching of the modal expansions is then performed at the subdomain interfaces according to fluid linearized inviscid conservation equations. A Kutta condition is also added at the blade/vane trailing edges. The resulting infinite system of equations is then truncated and the linear system inverted. This method has already been successfully applied to the two-dimensional sound generation and propagation in bifurcated channels as illustrated in the SDT benchmark case. It has also successfully modeled the sound propagation and generation in three-dimensional annular unstaggered flat plate cascades both for tonal⁵¹ and broadband noise as seen in the IDEALVENT rotor/statorcase. Further extensions not presented here are the unique trailing edge noise for annular unstaggered flat plate cascade,¹⁴ and the tonal wake interaction noise model for inhomogeneous stator vanes.⁵² Future developments will focus on providing a complete three-dimensional noise model with bifurcated channels for stator/OGV noise.

For CROR architectures characterized by low-solidity hardly overlapping blade rows, several extensions to Amiet's compressible isolated airfoil theory are proposed to account for most of the blade design features such as their high sweep. These airfoil responses are then seen as equivalent dipoles in a proper acoustic analogy, Curle for stationary airfoils and FWH for CROR blades, to yield both far-field tonal and broadband noise. For the tonal noise case, these unsteady loadings are applied to the mean camber surface of the blade and an interpolation step is performed to yield continuous phase and amplitude of these responses along the span (from strip to strip). The extended noise models are first shown to reproduce the turbulence interaction noise on swept airfoils well and to capture most of the features of a realistic CROR tonal and broadband noise at approach. In both cases, accounting for sweep is crucial to improving the comparison with experiments. Further extensions not presented here are the noise generation by the upstream pylon wake as shown in Figure 8, and the blade thickness and steady loading noise present at high speed.⁵³ Future developments will tackle the leading edge vortex noise and the junction noise. The former is always present in these highly swept blades as evidenced in the ECL experiment presented here, and a preliminary model has already been proposed by Jaouani et al.⁵⁴ The latter was also evidenced in the same experiment by beamforming and a preliminary model proposed by Giez et al.⁵⁵ In view of its versatility and possibilities of extension, Amiet's method appears as well suited for fast-running, parametric analytical open rotor noise predictions. Such predictions could then be used as part of an optimization tool dedicated to low-noise design.

Declaration of conflicting interests

The author(s) declared no potential conflicts of interest with respect to the research, authorship, and/or publication of this article.

Funding

The author(s) disclosed receipt of the following financial support for the research, authorship, and/or publication of this article: Most of the work presented here has been supported by the industrial Chair in Aeroacoustics at Université de Sherbrooke in Canada, and the industrial Chair ADOPSYS in France. The former is financed by Airbus, Safran Ventilation Systems, Valeo and Safran Aircraft Engines, and the latter is cofinanced by Safran Aircraft Engines and the French National Research Agency (grant ANR-13-CHIN-0001-01), which are all warmly acknowledged. This work was also partially performed within the framework of the Labex CeLyA of the Université de Lyon, within the program “Investissements d’Avenir” (grant ANR-10-LABX-0060/ANR-11-IDEX-0007) operated by the French National Research Agency.

References

1. Hughes C. *NASA collaborative research on the ultra high bypass engine cycle and potential benefits for noise, performance, and emissions*. Technical memorandum TM-2013-216345, NASA, Springfield, VA, 2013.
2. Ffowcs Williams JE and Hawkings DL. Theory relating to the noise of rotating machinery. *J Sound Vib* 1969; 10: 10–21.
3. Chu BH and Kovászny LSG. Non-linear interactions in a viscous heat-conducting compressible gas. *J Fluid Mech* 1958; 3: 494–514.
4. Daroukh M, Moreau S, Gourdain N, et al. Effect of distortion on turbofan tonal noise at cutback with hybrid methods. *Int J Turbomach Propuls Power* 2017; 2: 1–22.
5. Daroukh M, Moreau S, Gourdain N, et al. Complete prediction of modern turbofan tonal noise at transonic regime. In: *ISROMAC-17, International Symposium on Transport Phenomena and Dynamics of Rotating Machinery*, Maui, HI, 2017.
6. Glegg SAL. The response of a swept blade row to a three-dimensional gust. *J Sound Vib* 1999; 227: 29–64.
7. Posson H, Moreau S and Roger M. Broadband noise prediction of fan outlet guide vane using a cascade response function. *J Sound Vib* 2011; 330: 6153–6183.
8. Posson H, Beriot H and Moreau S. On the use of an analytical cascade response function to predict sound transmission through an annular cascade. *J Sound Vib* 2013; 332: 3706–3739.
9. Posson H and Peake N. The acoustic analogy in an annular duct with swirling mean flow. *J Fluid Mech* 2013; 726: 439–475.
10. de Laborderie J and Moreau S. Prediction of tonal ducted fan noise. *J Sound Vib* 2016; 372: 105–132.
11. Posson H, Roger M and Moreau S. On a uniformly valid analytical rectilinear cascade response function. *J Fluid Mech* 2010; 663: 22–52.
12. Grace SM. Fan broadband interaction noise modeling using a low-order method. *J Sound Vib* 2015; 346: 402–423.
13. Elhadidi B and Atassi HM. Sound generation and scattering from radial vanes in uniform flow. In: *Proceedings of ICFDP7, seventh international conference of fluid dynamics and propulsion*, Sharm El-Sheikh, Egypt, vol. AAC-3, 2001.
14. François B, Roger M and Moreau S. Cascade trailing-edge noise modeling using a mode-matching technique and the edge-dipole theory. *J Sound Vib* 2016; 382: 310–327.
15. Bouley S, François B, Roger M, et al. On a two-dimensional mode-matching technique for sound generation and transmission in axial-flow outlet guide vanes. *J Sound Vib* 2017; 403: 190–213.
16. Mittra R and Lee S. *Analytical techniques in the theory of guided waves*. New York, NY: The MacMillan Company, 1971.

17. Schram C, Christophe J, Shur M, et al. Fan noise predictions using scale-resolved, statistical, stochastic and semi-analytical models. In: *Twenty-third AIAA/CEAS aeroacoustics conference*, Denver, CO, paper no. 2017–3386, 2017.
18. Sack S and Abom M. Investigation of orifice aeroacoustics by means of multi-port methods. *J Sound Vib* 2017; 407: 32–45.
19. Roger M and François B. Combined analytical models for sound generation and transmission in cambered axial-flow outlet guide vanes. *Eur J Mech B/Fluids* 2017; 61: 218–225.
20. Roger M, Moreau S and Marsan A. Generation and transmission of spiral acoustic waves in multi-stage subsonic radial compressors. In: *Twentieth AIAA/CEAS aeroacoustics conference*, Atlanta, GA, paper no. 2014–3232, 2014.
21. Rienstra S. Sound propagation in slowly varying lined flow ducts of arbitrary cross-section. *J Fluid Mech* 2003; 495: 157–173.
22. Ovenden N. A uniformly valid multiple scales solution for cut-on cut-off transition of sound in flow ducts. *J Sound Vib* 2005; 286: 403–416.
23. Hixon R. Computational aeroacoustics prediction of acoustic transmission through a realistic 2D stator. In: *Seventeenth AIAA/CEAS aeroacoustics conference*, Portland, OR, paper no. 2011–2706, 2011.
24. Colin Y, Blanc F, Caruelle B, et al. Computational strategy for predicting CROR noise at low-speed. Part II: investigation of the noise sources computation with the chorochronic method. In: *Eighteenth AIAA/CEAS aeroacoustics conference*, Colorado Springs, CO, paper no. 2012–2222, 2012.
25. Zante DV and Envía E. *Prediction of the aero-acoustic performance of open rotors*. Technical report NASA-TM-2014-218132, NASA, Springfield, VA, 2014.
26. Soulat L, Kernemp I, Sanjosé M, et al. Numerical assessment of the tonal noise of counter-rotating open rotors at approach. *Int J Aeroacoust* 2016; 15: 23–40.
27. Colin Y, Carazo A, Caruelle B, et al. Computational strategy for predicting CROR noise at low-speed. Part I: review of the numerical methods. In: *Eighteenth AIAA/CEAS aeroacoustics conference*, Colorado Springs, CO, paper no. 2012–2221, 2012.
28. Schnell R, Yin J, Voss C, et al. Assessment and optimization of the aerodynamic and acoustic characteristics of a counter rotating open rotor. *J Turbomach* 2012; 134: 061016.
29. Lepot I, Leborgne M, Schnell R, et al. Aero-mechanical optimization of a contra-rotating open rotor and assessment of its aerodynamic and acoustic characteristics. *Proc IMechE, Part A: J Power and Energy* 2011; 225: 850–863.
30. Grasso G. *Development of hybrid methods for the computation of tonal and broadband fan noise source and propagation*. PhD Thesis, Université de Sherbrooke/von Karman Institute for Fluid Dynamics, Sherbrooke, Canada, 2017.
31. Hanson DB. Noise of counter-rotation propellers. *J Aircraft* 1985; 22: 609–617.
32. Kingan MJ. Open rotor broadband interaction noise. *J Sound Vib* 2013; 332: 3956–3970.
33. Amiet RK. Acoustic radiation from an airfoil in a turbulent stream. *J Sound Vib* 1975; 41: 407–420.
34. Amiet RK. Noise due to turbulent flow past a trailing edge. *J Sound Vib* 1976; 47: 387–393.
35. Roger M and Moreau S. Extensions and limitations of analytical airfoil broadband noise models. *Int J Aeroacoust* 2010; 9: 273–305.
36. Moreau S and Roger M. Competing broadband noise mechanisms in low-speed axial fans. *AIAA J* 2007; 45: 48–57.
37. Rozenberg Y. *Modélisation analytique du bruit aérodynamique à large bande des machines tournantes: utilisation de calculs moyennés de mécanique des fluides*. PhD Thesis, École Centrale de Lyon, Ecully, France, 2007.
38. Quaglia M, Moreau S, Roger M, et al. A three-dimensional analytical approach for open-rotor blade vortex interaction (BVI) tonal noise. In: *Twenty-first AIAA/CEAS aeroacoustics conference and exhibit*, Dallas, TX, paper no. 2015–2984, 2015.

39. Giez J, Vion L, Roger M, et al. Effect of the edge and tip vortex on airfoil self noise and turbulence impingement noise. In: *Twenty-second AIAA/CEAS aeroacoustics conference and exhibit*, Lyon, France, paper no. 2016–2996, 2016.
40. Quaglia M, Leonard T, Moreau S, et al. A 3D analytical model for orthogonal blade-vortex interaction noise. *J Sound Vib* 2017; 399: 104–123.
41. Roger M and Carazo A. Blade-geometry considerations in analytical gust-airfoil interaction noise models. In: *Sixteenth AIAA/CEAS aeroacoustics conference and exhibit*, Stockholm, Sweden, paper no. 2010–3799, 2010.
42. Roger M, Schram C and Moreau S. On vortex-airfoil interaction noise including span-end effects, with application to open-rotor aeroacoustics. *J Sound Vib* 2014; 333: 283–306.
43. Quaglia M. *Méthodes de prévision acoustique semi-analytiques pour un doublet d'hélices contra-rotatives isolé*. PhD Thesis, Université de Sherbrooke, Sherbrooke, Canada, 2017.
44. Hanson DB and Parzych DJ. *Theory for noise of propellers in angular inflow with parametric studies and experimental verification*. Technical report NASA-CR-4499, NASA, Springfield, VA, 1993.
45. Carazo A, Roger M and Omais M. Analytical prediction of wake-interaction noise in counter-rotation open rotors. In: *Seventeenth AIAA/CEAS aeroacoustics conference and exhibit*, Portland, OR, paper no. 2011–2758, 2011.
46. Quaglia M, Moreau S, Roger M, et al. A preliminary semi-empirical approach for CROR noise modeling. In: *Twenty-second AIAA/CEAS aeroacoustics conference*, Lyon, France, paper no. 2016–2743, 2016.
47. Blandeau V and Joseph P. Broadband noise predictions due to rotor-wake/rotor interaction in contra-rotating open rotors. *AIAA J* 2010; 48: 2674–2686.
48. Blandeau V, Joseph P, Kingan M, et al. Broadband noise predictions from uninstalled contra-rotating open rotors. *Int J Aeroacoust* 2013; 12: 245–282.
49. Casalino D, Avallone F, Gonzales-Martino I, et al. Aeroacoustic study of a wavy stator leading edge in a realistic fan/OGV stage. In: *ISROMAC-17, international symposium on transport phenomena and dynamics of rotating machinery*. Maui, HI, 2017.
50. Perez Arroyo C, Leonard T, Sanjose M, et al. Large Eddy simulation of a scale-model turbofan for fan noise source diagnostic. In: *ISROMAC-17, international symposium on transport phenomena and dynamics of rotating machinery*, Maui, HI, 2017.
51. Bouley S, François B and Roger M. On a mode-matching technique for sound generation and transmission in a three-dimensional annular cascade of outlet guide vanes. In: *Twenty-second AIAA/CEAS aeroacoustics conference and exhibit*, Lyon, France, paper no. 2016–2880, 2016.
52. Bouley S, Roger M and Finez A. Rotor-stator wake-interaction tonal noise modeling with an edge-dipole approach. In: *Twenty-second AIAA/CEAS aeroacoustics conference and exhibit*, Lyon, France, paper no. 2016–3061, 2016.
53. Jaouani N, Roger M, Node-Langlois T, et al. Analytical prediction of the pylon-wake effect on the tonal noise radiated by the front-rotor of CROR propulsion systems. In: *Twenty-first AIAA/CEAS aeroacoustics conference and exhibit*, Dallas, TX, paper no. 2015–2985, 2015.
54. Jaouani N, Roger M, Node-Langlois T, et al. Effect of a model leading-edge vortex on the blade aerodynamic response for application to CROR tonal noise predictions. In: *Twenty-second AIAA/CEAS aeroacoustics conference and exhibit*, Lyon, France, paper no. 2016–2744, 2016.
55. Giez J, Vion L, Roger M, et al. Effects of intermittency and geometry on the turbulence impingement noise of a CROR rear-rotor blade. In: *Twenty-third AIAA/CEAS aeroacoustics conference and exhibit*, Denver, CO, paper no. 2017–3217, 2017.